Eddy-Current Loss Analysis of Copper-Bar Windings of Ultra High-Speed PM Motor

Toshihiko Noguchi
IEEE Senior Member
Shizuoka University
3-5-1 Johoku, Naka-Ku, Hamamatsu, Shizuoka, Japan
E-Mail: ttnogut@ipc.shizuoka.ac.jp

Takehiro Komori
IEEE Student Member
Shizuoka University
3-5-1 Johoku, Naka-Ku, Hamamatsu, Shizuoka, Japan
E-Mail: f0330112@ipc.shizuoka.ac.jp

***Abstract*—** This paper describes a loss analysis of an eddy current generated in the copper-bar windings of a 1.5-kW, 150,000-r/min PM motor fed by a 12-V power supply, which is applicable to an automotive supercharger. The proximity effect in the winding conductors is a result of the eddy-current caused by the magnetic fields generated by the neighboring conductors. The analysis results show that the proximity losses can be significantly reduced by an appropriate magnetic shielding and segmentation of the conductors.

Keywords—*«high speed drive», «permanent magnet motor», «adjustable speed drive», «automotive supercharger»,«automotive component».*

I. INTRODUCTION

A supercharger is an auxiliary machine to enhance the output power of a combustion engine and to reduce the engine displacement simultaneously. Employing the supercharger is also effective to improve the combustion efficiency, the exhaust gas quality and the engine torque response. The conventional supercharger has a mechanical linkage with the engine, and it compresses inlet air into the engine cylinders by means of the mechanical power provided by the crank shaft. Figure 1 (a) illustrates a mechanical configuration of the conventional supercharger. As shown in the figure, many of the superchargers employ a displacement compressor because its operation speed is limited by a low revolution speed of the engine. However, the displacement compressor has drawbacks such as lower efficiency and lower boost pressure, compared with a centrifugal compressor, which prevents further performance improvement of the supercharging system. In order to solve these problems, electrification of the supercharger is significantly important and is very promising approach as a next-generation auxiliary machine system. Figure 1 (b) shows an outline of the electrically operated supercharger where an ultra high-speed permanent magnet (PM) motor is used to drive the centrifugal compressor instead of the displacement compressor. Since the electrically operated supercharger allows use of the centrifugal compressor and achieves a mechanical-linkage-free system, many advantages are obtained, e.g., more efficient operation, higher rotation speed, higher boost pressure, faster response of the inlet air compression, and smaller mechanical dimensions than those of the conventional displacement compressor based system. Furthermore, such a mechanical-linkage-free system gives freedom of the mechanical design around the engine, and makes it possible to reduce overall mechanical losses as well as to eliminate the complicated linkage mechanism.

This paper discusses an optimum design of the ultra high-speed PM motor of which specific application is the electrically operated supercharger of the automotive engine. The motor is fed by a three-phase inverter with a 12-V battery as a DC power supply; thus the motor design must meet a high-current and high-frequency operation requirement without sacrificing the motor efficiency and the power density. The investigated motor has a rated output power of 1.5 kW and the maximum rotation speed of 150,000 r/min, respectively. In order to achieve this goal, various technical issues must be solved, e.g., drastic reduction of the synchronous impedance, minimization of the iron and the copper losses, further improvement of the motor efficiency and

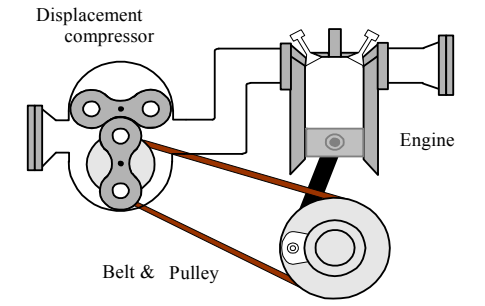

(a) Conventional system.

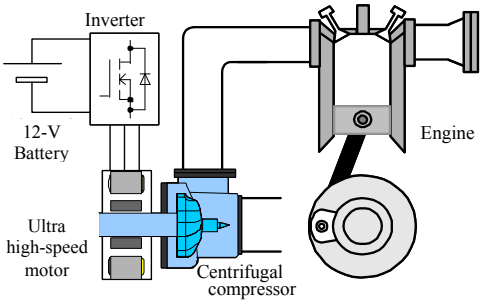

(b) Electrically operated system.

Fig. 1. System configurations of conventional and electrically operated supercharging systems.

Table 1. Design target of ultra high-speed PM motor.

Assumed engine	1.5 L class
Rated output power	1.5 kW
Rated speed	150,000 r/min
Rated torque	0.0955 Nm
Overload and duration	3kW (200 % over load) for 1 s

the power density, mechanical stabilization in high-speed operation range, and so forth. In addition, these electrical design requirements must be satisfied all together with a compact and robust mechanical design. On the way of optimization process in the machine design, a finite element method (FEM) based electromagnetic field analysis is conducted to make fine-tuning of the detailed motor shape and to maximize the efficiency and the power density at the same time. In this paper, the eddy current in the copper-bar windings and the proximity effect caused by the eddy current are focused on.

II. Required Specifications of Ultra High-Speed PM Motor

Assuming a 1,500-cc class automotive engine, the ultra high-speed PM motor is required to have the rated power of 1.5 kW at the maximum rotation speed of 150,000 r/min to achieve the electrically operated supercharging system. When boosting the inlet air pressure extremely fast response is required because the compressor must be accelerated from several ten thousand r/min to the maximum rotation speed in approximately 0.5 s, which surpasses a response time of the conventional supercharger. In order to meet this requirement, the motor must have a short-duration overload capacity, which is a double of the rated output power for 1 s. Table I shows target specifications of the motor determined by the above requirement.

III. Basic Design Concept of Ultra High-Speed PM Motor

In order to achieve the highest efficiency and the highest power density among varieties of the electric motors, a two-pole three-phase surface permanent-magnet synchronous motor (SPMSM) is focused on as the best choice for the ultra high-speed motor drive because of the simple rotor structure and no magnetizing current, which implies higher efficiency than other motors. The stator has a six-tooth six-slot structure and the concentrated windings, which is remarkably effective to reduce the copper loss and the leakage inductance thoroughly as well as the synchronous inductance. Each phase has a pair of the double-turned windings in parallel, and the windings are not ordinary wires but copper bars whose shape is like an alphabetical letter “b.” It is necessary to reduce as much stator iron loss as possible even at 150,000 r/min operation, so high-performance 6.5-% silicon electromagnetic steel plates whose thickness is only 0.1 mm are employed to compose a laminated stator iron core.

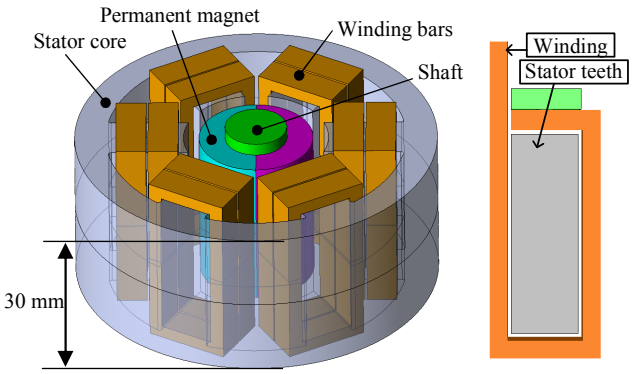

Fig. 2. Analysis model with two-turn windings.

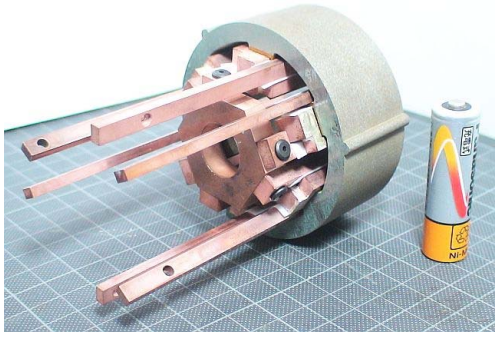
Fig. 3. Stator iron core with two-turn windings.

Table 2. Design parameters of ultra high-speed PM motor.

Motor type	Surface Permanent Magnet Synchronous Motor (SPMSM)
Number of phases	Three-phase
Number of poles	2 poles
Stator configuration	Concentrated winding structure
Winding configuration	2 turns, 2 parallels per phase
Electromagnetic steel plates	10JNEX900 (0.1-mm thick, 6.5-% silicone, μ_s=23000, B_{max}=1.8 T)
Permanent magnet	N-39SH Nd-Fe-B (B_r=1.28 T, ${}_BH_c$=955 kA/m, BH_{max}=310 kJ/m^3)
Bearings	Angular ceramic-ball bearings with grease lubrication

On the other hand, the rotor consists of a Nd-Fe-B permanent magnet and a molybdenum alloy shaft. Use of the Nd-Fe-B permanent magnet allows not only motor efficiency improvement but also drastic reduction of the rotor size and the inertia. In addition, such a strong Nd-Fe-B permanent magnet that has BHmax = 310-kJ/m3 makes it possible to widen the air gap, which is essential to reduce the synchronous inductance and to obtain a sinusoidal electromotive force (e.m.f.) regardless of the concentrated stator winding structure. Table II is a summary of the basic conceptual design parameters of the ultra high-speed PM motor to be investigated in this paper.

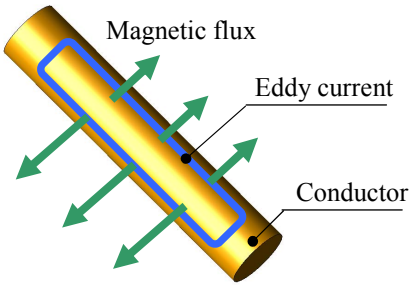

(a) Strand eddy current in single conductor.

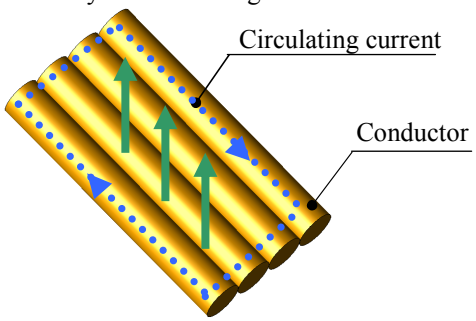

(b) Circulating current

Fig. 4. Eddy current loss mechanism in conductor.

IV. Eddy Current Loss Generated in Conductors by Interlinkage of Flux

The strong permanent magnet is very effective to widen the air gap, which is indispensable to reduce the synchronous inductance. On the other hand, when the rotation speed is increased, a leak magnetic flux cannot be ignored due to the widened air gap. Possible loss factors in addition to the iron loss and the copper loss are the eddy-currents in the conductors of the motor windings as follows;

(1) strand eddy currents (circulating currents within individual wire strands), and

(2) bundle proximity currents (circulating currents between different strands of the same wire bundle).

In general, the leakage magnetic flux is classified in the following three classes; a) main flux by the permanent magnet. b) leakage magnetic flux generated in the vicinity of the air gap, and c) slot leakage magnetic flux generated between a front end opening and a bottom portion of the slot. The external field in the slot arises from the slot leakage flux crossing between the slot walls combined with the fringing flux emanating from the slot opening. A stator magnetic flux substantially flows in a diameter direction in the tooth. Therefore, the leakage magnetic flux generated in the slots is rather small. However, in the case of the motor with a large air gap, the leaked magnetic flux generates an eddy current in the conductors. Figure 4 shows a conceptual illustration of the eddy current loss mechanism in the conductors. Figure 4 (a) shows the eddy current in a single conductor. An external AC field induces the eddy current inside each strand as a result of Faraday's law. This eddy current flows so that they tend to generate a flux, that disturbs changes of the magnetic field.

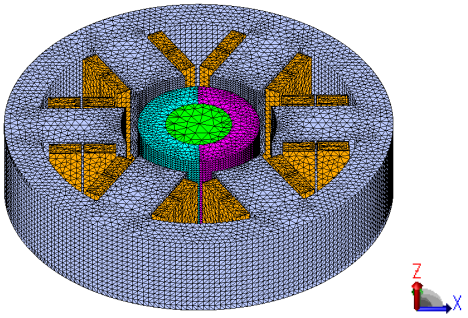

Fig. 5. Mesh division (1/2 model) of analysis model.

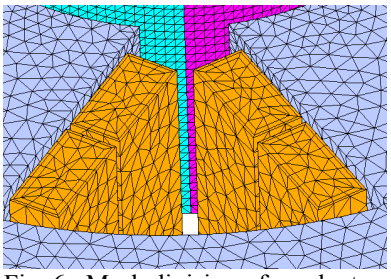

Fig. 6. Mesh division of conductor.

Figure 4(b) shows a circulating current between the different strands. Assuming that the shorted strands in the slot are not connected to any external circuit, the total slot current in the presence of an external ac field must be zero but the individual strands can experience non-zero currents because of the circulating current. On the other hand, if the slot strands are connected to an external circuit, the total current in the conductors can be attributed to a superposition of the externally-applied armature current and the effects of an external magnetic field. Bundle proximity current is dependent of the magnetic flux interlinked with the different strands and the impedance of the circuit network by the strands. By using transposed strands in a slot, it is possible to roughly equalize the strength of the magnetic field received by the strands in the slot. Thus, the voltage induced in the different strands is cancelled and becomes zero. For these reasons, the circulating current is not caused as a principle.

V. Specifications of Analysis Model

The purpose of this paper is to investigate the effects of the magnetic shielding and the segment conductors on the strand proximity losses in the stator windings of the ultra high-speed motor by using a three-dimensional finite element method (3-D FEM) analysis. Figures 5 and 6 illustrate a half portion of the generated mesh (993033 elements and 309961 nodes in the whole mesh) and a mesh of the conductors, respectively. Besides, it is analyzed at 2-degree angle intervals. In addition, the mesh of the conductors are suitable for loss evaluation because it is possible to calculate the deviation of the magnetic flux distribution due to the skin effect. Modeling of the coil end allows to visualize current path of the strand eddy current and to evaluate the eddy current loss that arises within the specified strand.

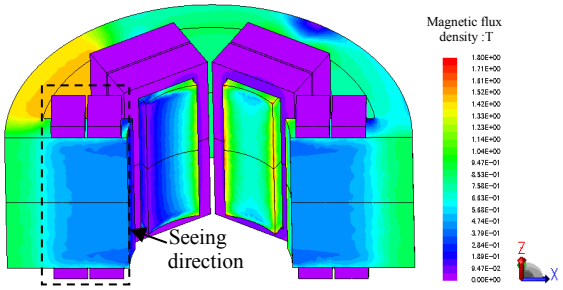

Fig. 7. Magnetic flux density distribution (birds-eye view)

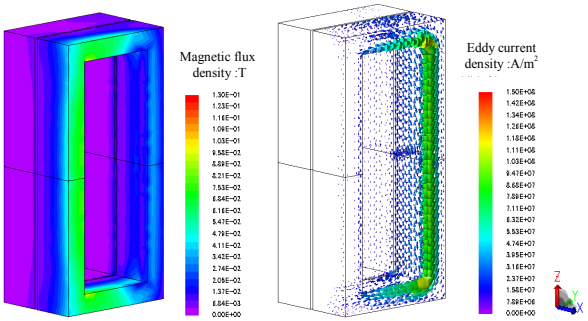

(a) Magnetic flux density. (b) Eddy currents density.

Fig. 8. Magnetic flux density and eddy current density in conductor.

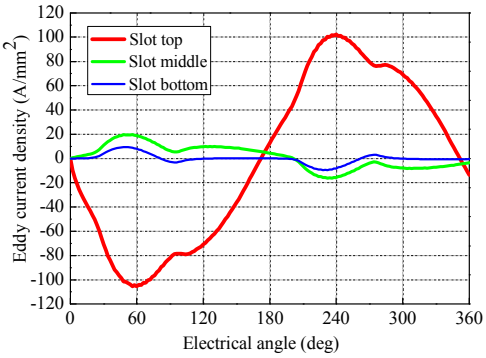

Fig. 9. Eddy current density in conductor. (Z-axis directions)

In order to emphasize the effects of the eddy current in the copper-bar windings, the permanent-magnet thickness is changed from 3.75mm to 5mm, compared with the machine shown in Fig. 3 to investigate the effects of the magnetic shielding and the segment conductors more accurately.

VI. Analysis Results

A. *Analysis of benchmark model*

Figure 7 represents an example of the resultant magnetic-flux density distribution at 150,000 r/min. The rotor position is 60 deg. As shown in the result, the maximum value of the magnetic flux density in the back yoke is approximately 1.4 T; thus, the significant magnetic saturation is hardly observed in the iron core. Figure 8 shows the magnetic flux density distribution and the eddy current density distribution at 150,000 r/min under the condition of 0 A of the conductor current in the slot. From the analysis, it is confirmed that the

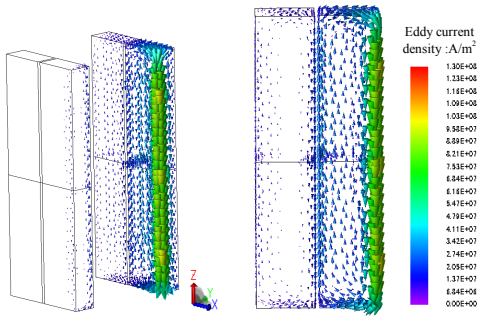

Fig. 10. Eddy current density in conductor.

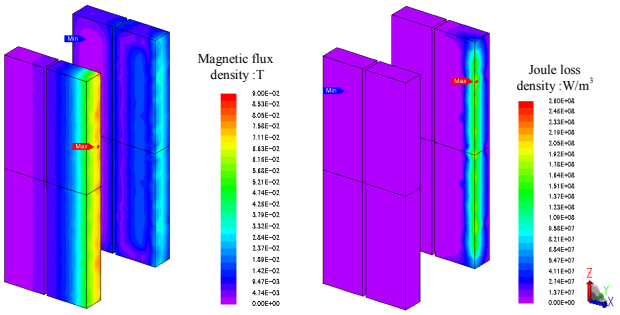

(a) Magnetic flux density. (b) Loss density.

Fig. 11. Magnetic flux density and loss density in conductor.

eddy current is generated in the conductor by interlinkage of the leakage magnetic flux. Figure 9 shows the eddy current density in a z-axis direction at different winding positions at 150,000 r/min. The measured positions of the eddy current density are set in area closest to the tooth of the iron core. It can be seen that the eddy current loss are concentrated at the edge of the top conductor which may create the hot spots. Figure 10 shows the eddy current density distributions when the coil ends have been eliminated. It can be found that the eddy current concentrates at the edge of the top conductor closest to the tooth. It is possible to confirm the eddy current caused by a circumferential-direction component of the magnetic flux as well as the eddy current caused by a diameter-direction component. Thus, the direction of eddy current flowing in the conductor depends on the time variation of the magnetic leakage flux. Figure 11 shows the magnetic flux density distribution and the eddy current density distribution in the conductor. Figure 11(a) shows that the slot leakage field level is the highest in the slot opening region and the lowest in the slot bottom region. Figure 11(b) also shows that the loss density is the highest in the conductor located in the slot opening region, while it is the lowest in the conductor located in the slot bottom region. These results show that the eddy current loss is approximately proportional to the square of the slot leakage magnetic field.

B. *Effect of magnetic shielding*

Figure12 shows five analysis models for evaluation of the magnetic shielding. Each tooth shape is as follows, (a) straight-shape tooth tip, (b) chamfering-shape tooth tip, (c) square-shape tooth tip, (d) trapezoidal-shape tooth tip, and (e) bridge-shape tooth tip. Figure 13 shows the eddy current loss

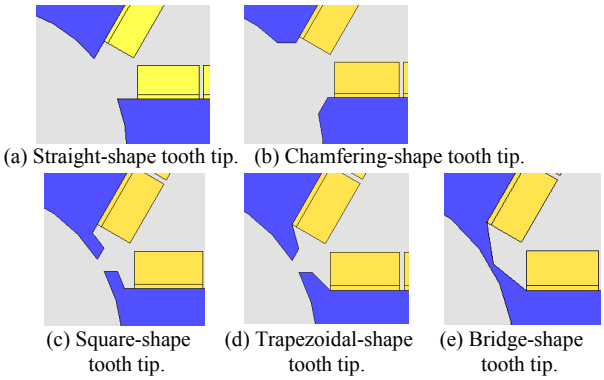

Fig. 12. Teeth shapes for comparative study.

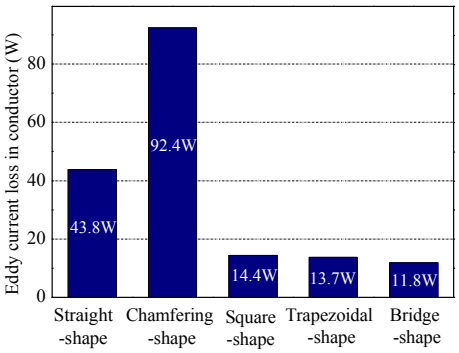

Fig. 13. Eddy current losses in conductor with respect to teeth shapes.

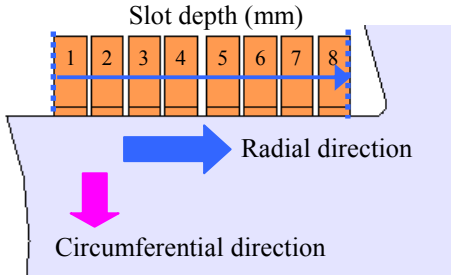

Fig. 14. Positional relation between segment conductors in slot and slot depth.

comparison result in the conductor with respect to the teeth shapes. In the case of the straight-shape tooth tip, the leakage magnetic flux interlinked with the conductor increases because the flange portion is not formed at the end of the tooth. In the case of the chamfering-shape tooth tip, as the leakage magnetic flux interlinked with the conductor is detrimentally increased in comparison with those in the straight-shape tooth tip, the eddy current loss remarkably increases. In addition, it is found that the flange can reduce the leakage of the magnetic flux from the rotor magnet to the conductors, and the eddy current loss can be effectively reduced by employing the tooth tips for the magnetic shielding.

C. *Magnetic flux density in conductor with respect to slot depth*

Figure 14 shows the relationship between the segment conductor in a slot and the slot depth. Figure 15 shows the

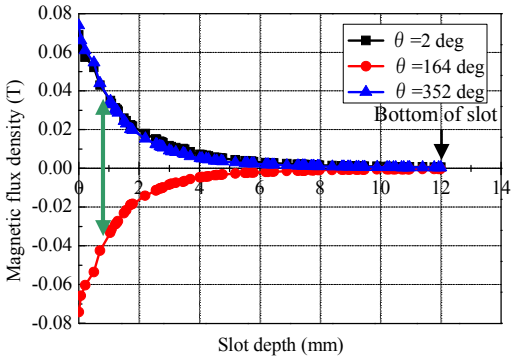

Fig. 15. Magnetic flux density in conductor with respect to slot depth.

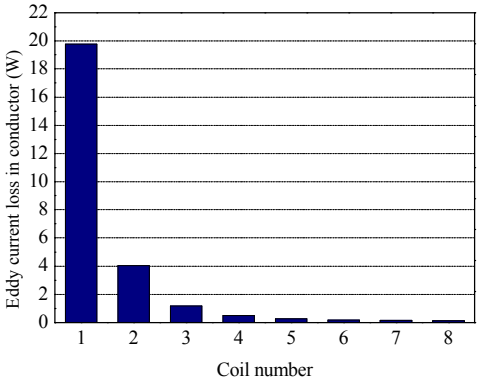

Fig. 16. Eddy current loss in segment conductor.

magnetic flux density in the conductor with respect to the slot depth, which corresponds to the change of the rotation angle. The magnetic flux density in the conductor gradually decreases from 2 deg according to the rotation angle, and becomes the minimum value at 164 deg and the maximum value at 352 deg. Thus, the eddy current loss is increased because the first coil part at the tip is arranged in the vicinity of a portion where the magnetic flux density variation appears to be the greatest in the magnetic circuit. In the conductor at the bottom of the slot, the magnetic leakage flux hardly varies, which means almost no eddy current flows through the conductor. Figure 16 shows the eddy current loss of the layers in the segment conductor. From this result, it is confirmed that the first coil part at the tip occupies a dominant part of the eddy current loss. Thereby, the eddy current loss in the coil can be largely reduced when the conductor is placed at the bottom of the slot.

D. *Effect of segmentation of conductor*

The Segment conductor is formed in one strand with a prescribed cross-section by combining a plurality of divided element wires. The cross-sectional area of the conductor is split into multiple radial widths corresponding to the radial position. Figure 17 shows the eddy current density distribution and loss density distribution in the conductor divided in four cross sectional. It is confirmed that the eddy current density is reduced because of by dividing the conductors having small cross sectional area. Figure 18 shows corresponding relationship between the eddy current loss and the number of

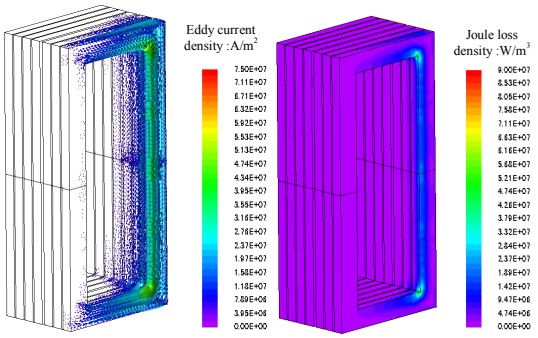

(a) Eddy current density. (b) Loss density.

Fig. 17. Eddy current density and loss density in segment conductor.

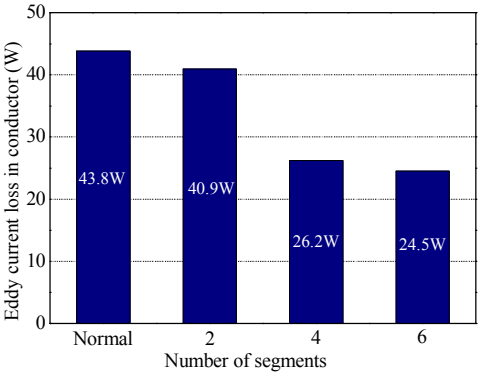

Fig. 18. Number of segments and eddy current loss in segment conductor.

the divided the segments. In the case of dividing to two conductors, it is small in the rate of decrease of the eddy current loss compared to segment-less conductor. This is because of locally concentrating the eddy current generated at top of the segment conductor. Thus, the windings of slot top is divided into the segment conductor by division widths corresponding to the magnetic flux density change ratio at different the segments conductor position, and the eddy current loss generated in each the segment conductor is suppressed. Figure 19 shows 150 A peak phase current at 150,000 r/min and 1 r/min. In the case of dividing to two conductors, it is possible to confirm an uneven distribution of the current density between the first coil and the second coil. Figure 20 shows the total loss in the conductor with respect to the rotational speed. It is confirmed that the loss due to nonuniform current density is increased in proportion to the rotational speed.

VII. Conclusion

This paper described the mechanism of inducement of the strand eddy current and the circulating current generated in copper-bar windings by interlinkage of the magnetic flux. In addition, it is found through 3D-FEM analysis that the eddy current loss of the conductor is reduced by the magnetic shielding and the segment conductors. The prototype shown in Fig. 3 will be experimentally examined in detail in the future works.

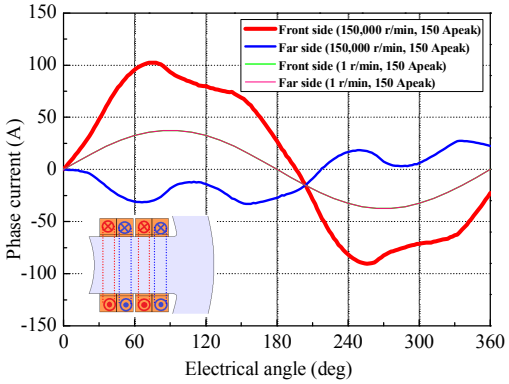

Fig. 19. Phase current.

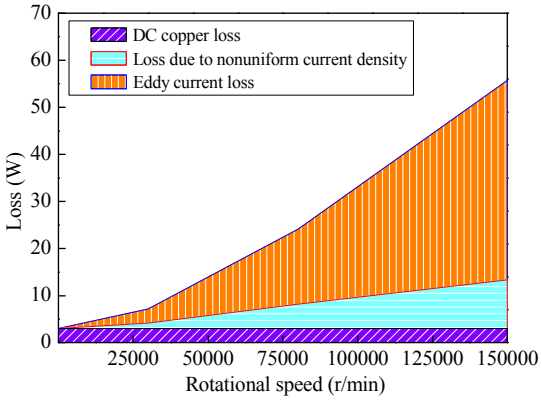

Fig. 20. Total loss in conductor.

References

[1] M. Okawa, "Design Manual of Magnetic Circuit and PM Motor," Sogo Research, 1989 (in Japanese).

[2] T. Noguchi, Y. Takata, Y. Yamashita, Y. Komatsu, and S. Ibaraki, "220000r/min, 2-kW Permanent Magnet Motor Drive for Turbocharger", IEE-Japan International Power Electronics Conference (IPEC2005) -Niigata,p.p. 2280-2285, 2005.

[3] C. Zwyssig, M. Duerr, D. Hassler, and J. W. Kolar, "An Ultra-High-Speed, 500000 rpm, 1 kW Electrical Drive System," The Fourth Power Conversion Conference

[4] T. Noguchi, and M. Kano, "Development of 150000r/min, 1.5kW Permanent-Magnet Motor for Automotive Supercharger," The Seventh International Conference on Power Electronics and Drive Systems (PEDS2007) Bangkok, 2A-03, 2007

[5] P. B. Reddy, T. M. Jahns and T. P. Bohn, "Transposition Effects on Bundle Proximity Losses in High-Speed PM Machines," IEEE Ind. Appl. Soc Annual Meeting, 2009, pp 1919-1926.

[6] T. S. Iwasaki, R. P. Deodhar, Y. Liu, A. Pride, Z. Q. Zhu and J. J.Bremner, "Influence of PWM on the Proximity Loss in Permanent-Magnet Brushless AC Machines," IEEE Trans. on Ind. Appl., vol. 45,No. 4, 2009, pp 1359 - 1367

[7] Popescu, M, Dorrell, D.G., "Skin effect and proximity losses in high speed brushless permanent magnet motors," Energy Conversion Congress and Exposition (ECCE), 2013, pp 3520 - 3527